

Prediction of new sp^3 silicon and germanium allotropes from the topology-based multiscale method

Vladimir A. Saleev* and Alexandra V. Shipilova†

*Department of Physics, Samara National Research University - 34,
Moskovskoe shosse, Samara, 443086, Russian Federation*

Davide M. Proserpio‡

*Università degli Studi di Milano, Dipartimento di
Chimica - via Golgi, 19, 20133 Milano, Italy and
Samara Center for Theoretical Materials Science (SCTMS),
Samara National Research University - 34,
Moskovskoe shosse, Samara, 443086, Russian Federation*

Giuseppe Fadda§

*Research and Education Center for Physics of Open Nonequilibrium Systems,
Samara National Research University - 34,
Moskovskoe shosse, Samara, 443086, Russian Federation*

Abstract

This article continues our recent publication¹ in which we have presented a comprehensive computational study of sp^3 carbon allotropes based on the topologies proposed for zeolites. Here we predict six new silicon and six new germanium allotropes which have similar group symmetries and topologies as those predicted for the early carbon allotropes, and study their structural, elastic, vibrational, electronic, and optical properties.

PACS numbers: 62.20.-x, 71.20.-b, 78.30.Am, 78.40.Fy

I. INTRODUCTION

In recent years, carbon allotropes have been the focus of an intense research activity (see 1 and references therein); among the methods used to find new potentially interesting allotropes, many are now well-known to physicists, such as evolutionary algorithms^{2,3}. The topological method used in Ref. 1 stems from a radically different philosophy, namely starting from well-known structures (instead of looking for new ones), extracting the connectivity of their fundamental building blocks (see 4 and 5 and references therein), and then replacing the latter by any other elementary structure; for instance in Ref. 1, silicates and zeolites were used as starting structures, their building blocks being obviously the silicon tetrahedra SiO_4^{4-} , the new elementary structures atoms of carbon (in 1) or silicon or germanium (in the present paper). Once done, the newly-found structures are relaxed; as the number of known zeolites and silicates is of the order of several hundreds of thousands^{6,7}, some filtering procedure (described in 1 and § II) is necessary.

Because of the chemical similarity of Si and Ge with C, as of course all of them belong to Group 14 (IUPAC nomenclature), it seemed a natural idea to extend the previous study to silicon and germanium. But instead of focusing on structural and mechanical properties only, we have emphasized here the generic physical properties of the allotropes (§ IV), including a discussion of the electronic, dielectric, optical, and vibrational properties.

Theoretical prediction of silicon and germanium allotropes is a subject of great interest because of their potential use in the semiconductor industry. Very recent works devoted to the silicon and germanium allotropes were aimed at finding prospective structures for photovoltaic applications, as silicon still keeps the leading position there (see for instance 8 and 9 and references therein). Several novel metastable phases of sp^3 -bonded silicon, obtained through a structural search based on carbon analogues as well as on random-structure searching approaches, were predicted¹⁰⁻¹⁷. Their total energy remains within 0.15 eV per atom from diamond silicon, and the band gaps are located between 1 and 1.5 eV; some of these structures have shown good absorption properties of solar light. Here we study 5 previously unknown sp^3 allotropes of silicon and germanium which are within 0.05 eV of the diamond phases, making them more energetically feasible; the sixth structure investigated here, namely #28, suggested in our previous work as a carbon allotrope, has already been studied as a phase of silicon and germanium in Ref. 15.

Another interesting conclusion of the present work is that distorted structures induce a severe reduction in s - p overlap, which might even provide for a metallic phase of germanium as discussed recently for some novel metastable phases of germanium¹¹.

II. APPROACH FOR STRUCTURE SEARCHING

A. Methodology

Details are given in 1; here we provide the necessary information. The topological analysis of many of the carbon allotropes found using a variety of methods (see 1 and references therein) has shown that they are generally related to silicates or zeolites; the idea was thus to start from the latter structures (of which hundreds of thousands are known) and by contracting the oxygen links in the Si–O bonds, to generate a large number of tetrahedral Si nets. The problem was then to filter among these structures the ones which could be interesting: the 3- and 4-ring nets were discarded (in order to avoid excessive strain in the silicon structures), the rest then submitted to a geometrical post-screening (mainly based on the nearest and next-to-nearest distances between Si atoms); progressively more refined methods (first classical potentials, then tight-binding) were used to determine the most favorable structures, and diamond- and lonsdaleite-related nets were rejected on the basis of their popularity in the literature^{18,19}. The final set consisted of the six structures with lowest energy #26, #27, #28, #50, #55, and #88, which are the object of the present paper. The optimized crystal structures of the predicted silicon allotropes are shown in Fig. 1; the germanium allotropes are not shown as they are very similar.

B. Nomenclature

The structures studied here, as already discussed above, are the same studied in Ref. 1, and are part of the SACADA (SAmara Carbon Allotrope DAtabase)^{20,21}: see Table I for the correspondence. The labels used in the present paper are the last two digits of the corresponding hypothetical zeolite structures in the Deem database⁶.

Present work	SACADA	Present work	SACADA
#26	4 ⁸ T15	#27	4 ⁸ T16
#28	4 ⁶ T17	#50	4 ⁷ T12
#55	4 ⁶ T16	#88	4 ⁶ T18

TABLE I. Correspondence between the labels used in the present paper and those used in SACADA for the equivalent carbon allotropes

III. COMPUTATIONAL METHODOLOGY

The main part of the computations, that is all electronic, dielectric, vibrational, and mechanical properties, plus the Raman shifts and infrared absorption spectra, was done with the CRYSTAL14 package^{22,23}, following the same methodology of Ref 1. The generalized-gradient approximation (GGA) and the Perdew-Burke-Erzenhof (PBE)²⁴ parameterizations for the exchange-correlation term were adopted; the basis set used is the triple- ζ valence with polarization (TZVP) as developed by Peitinger et al.²⁵. Structural relaxation was done using the conjugate gradient method; convergence was deemed achieved for forces below $3 \text{ meV } \text{\AA}^{-1}$ and stresses below 0.02 GPa. As to the Brillouin Zone (BZ), the usual Monkhorst-Pack sampling²⁶ was used and tested for convergence; the Shrinking Factors for the k -point generation for the unit cell and for $2 \times 2 \times 2$ supercells are $\{8, 8, 8\}$ and $\{4, 4, 4\}$ respectively. Raman shift spectra were computed for polycrystalline powder as implemented in the CRYSTAL14 package.

For the computations of the complex refractive indices and dielectric tensors in the visible and ultraviolet (UV) regions we used the VASP package instead^{27,28}. A plane-wave basis set with a cutoff energy of 500 eV and 350 eV for Si and Ge respectively was used throughout the calculations. For the basic ground-state properties the GGA-PBE was selected and the integration over the BZ performed using Monkhorst-Pack grids of $7 \times 7 \times 7$ k -points. For optical properties, we also used within both CRYSTAL14 and VASP the screened Heyd, Scuseria, and Ernzerhof (HSE06)²⁹ hybrid functional.

In order to ascertain the quality of the present computational approach, we have performed for the diamond structure a check on all the computed properties. As can be seen in Table II, the adopted method gives a fair agreement with experiment for the basic prop-

erties, including the band gap and the bulk modulus (two well-known issues of GGA-PBE); as to the computed optical properties of diamond Si and Ge and the details regarding the adopted methodology, see § IV E.

IV. RESULTS

A. Energetics of the various allotropes

For the basic computations (made at 0 K), the enthalpy is the thermodynamic potential:

$$H(V) = E(V) + p(V) \times V. \quad (1)$$

After calculation of the crystal energy E as a function of the volume V (see Figs. 2 and 3), we fit this dependence using the Birch-Murnaghan equation of state³⁰ to find the $p(V) = -\frac{dE}{dV}$ dependence and the differences of enthalpies $\Delta H(p) = H_X(p) - H_{dia}(p)$ between phase X and diamond as a parametric function of pressure p . As seen in Figs. 4 and 5, none of the new allotropes can be considered high-pressure variants, exactly as for carbon: indeed the difference with the diamond structure increases with pressure.

At zero pressure and non-zero temperature T , the Gibbs free energy is the thermodynamic potential:

$$F(T) = E(0) + E(T) - T \times S(T), \quad (2)$$

where $E(0)$ is the crystal energy at $T = 0$, $E(T)$ the thermal energy and $S(T)$ the entropy. $E(T)$ and $S(T)$ can be calculated in the quasi-harmonic approximation (see 31 for details of implementation in the CRYSTAL14 package). To calculate the entropy and thermal energy as a function of temperature, the phonon frequency spectrum of crystal has to be calculated:

$$S(T) = k_B T \left(\frac{\partial \log Q}{\partial T} \right)_{V,N} + k_B \log Q, \quad (3)$$

$$E(T) = k_B T^2 \left(\frac{\partial \log Q}{\partial T} \right)_{V,N}, \quad (4)$$

where $Q = \sum_j \exp(-E_j/k_B T)$ is the canonical partition function.

We have performed these frequency calculations using a $2 \times 2 \times 2$ supercell. We find that, contrary to the pressure dependence, the predicted Si and Ge allotropes may be high-temperature variants (see Fig. 6 for two examples of Si#26, Si#27 and Ge#26, Ge#27 allotropes), but because of the limitations of the quasi-harmonic method adopted here, it

cannot be ascertained whether this is the case or not, as the temperatures of transition are quite close to the melting temperature of silicon and germanium (resp. 1687 and 1211 K at $p = 101\,325\text{ Pa}$, see Ref. 32).

B. Mechanical properties

Silicon and germanium are not expected to exhibit mechanical properties of interest; nevertheless, it is necessary to compute the elastic constants C_{ab} in order to check the stability of the new allotropes against strain: all of them were found to be stable according to the Cauchy-Born criterion, i.e. the generic necessary and sufficient criterion that all eigenvalues of matrix C_{ab} be positive^{33,34}. The elastic constants are presented in the Supplementary Material. The bulk moduli are remarkably similar and systematically lower than the (already low) value for the diamond structure. Exactly as for the diamond structure, Ge allotropes exhibit lower bulk moduli B than their Si equivalents because of longer bonds, implying a lower electronic bonding density³⁵. The present allotropes exhibit a small mechanical anisotropy, either in pure extension or in shear or both; only structures #55 and #88 are slightly more compressible along the [100] crystallographic axis, somewhat reminding lonsdaleite (see below). The computed shear moduli G are also lower than for diamond: whereas for germanium the B/G ratio remains close to 1.35 (diamond Ge: 1.38), it is significantly higher for the Si allotropes (1.7 against 1.47 for diamond Si), at the limit of the Pugh threshold of 1.75 distinguishing brittle (low values of B/G) from ductile materials³⁶ (see however Ref. 37). In the same way, the Poisson ratio rises to 0.25-0.26 for the Si allotropes (0.22 for diamond Si), which is generally interpreted as another sign of increasing ductility³⁷, while remaining around 0.2-0.21 for Ge (0.21 for diamond Ge): the variance between Si and Ge is thus significantly larger for the new allotropes than for diamond. The bulk and shear moduli for the predicted silicon and germanium allotropes are accumulated in the Tables III and IV. The shear moduli were calculated via the elastic constants C_{ab} using the Voigt prescription³⁸. The bulk moduli were calculated from the equations of state as well as from the elastic constants, with very close resulting values.

As Ge bonding electrons are more delocalized than their Si counterparts in all the investigated allotropes (as can be seen for instance in plots of electronic charge densities or of the Electron Localization Function^{39,40}, not shown here), bonds in Ge are more susceptible

to angular deformation and correspondingly the shear moduli (measuring the resistance to shape changes) of the Ge compounds are always smaller than those of their Si equivalents (see for instance Ref. 35). From that point of view, Ge is indeed truly intermediate between C and Si (covalent bonding, strongly localized electrons) and Sn and Pb (metallic bonding, highly delocalized electrons). Consequently, the distortion to pure sp^3 bonding has more effects on Si allotropes.

C. Vibrational properties

Figs. 7 and 8 show (for structure #28; see Supplementary Material for the others) the phonon spectra and Density of States (DOS) in the BZ: no instabilities were found. As expected, the lowest dominant frequency is higher for Si than for Ge, as the latter atom is heavier (72.63 against 28.08 g mol⁻¹); if provisions are made for the different masses, the spectra are actually quite similar. The predominance in the DOS of high-frequency modes indicates that bond-bending modes are favored over bond-stretching; this is confirmed by the value of the Kleinman parameter⁴¹:

$$\zeta = \frac{C_{11} + 8C_{12}}{7C_{11} + 2C_{12}}, \quad (5)$$

which is low for all the allotropes (0 corresponding to bond-bending, 1 to bond-stretching modes), especially for Ge (some Si allotropes reach a value of $\frac{1}{2}$ and thus exhibit both modes), see the discussion at the end of the previous paragraph. Notice also that these high-frequency modes exhibit even lower dispersion across the BZ than diamond.

Closely connected to phonons are the Raman shift spectra (see Fig. 10); the Si structure retains the complicated spectrum of the C equivalent (see 1), whereas Ge has a far simpler spectrum. In substance, as symmetry is the same in both cases, the same vibrational modes are Raman-active (recall that diamond has by symmetry only one Raman-active mode); however, for C and Si allotropes, the derivative of the electronic polarisability is clearly higher, i.e. the (static) electronic contribution to the dielectric matrix is more susceptible to variations in atomic positions; notice that defective diamond⁴² shows a very similar Raman spectrum. If for carbon this is a direct consequence of the very short bonds (between 1.5 and 1.6 Å), this mechanism cannot be invoked for Si with respect to Ge, as bonds have basically the same lengths (2.4-2.6 against 2.3-2.4 Å for Si). As a consequence, the experimental

characterization of the Ge allotrope should be easy (a single shift), whereas it would be quite difficult for C or Si allotropes.

Contrary to the ideal diamond structures of silicon and germanium, the predicted allotropes absorb IR radiation, as shown in Fig. 10 for silicon and germanium allotropes #26 (see Supplementary Material for the others). The absorbance spectrum $I(\nu)$ is calculated according to the following classical absorption formula, averaged over the inequivalent polarization directions ii :

$$I(\nu) = \frac{1}{3} \sum_{ii=1}^3 \frac{4\pi}{\lambda\rho} \text{Im} [n_{ii}(\nu)] \quad (6)$$

where λ is the wavelength of the incident beam, ρ the crystal density of mass per unit volume and $n_{ii}(\nu)$ the complex refractive index, which is obtained via the real and imaginary parts of the complex dielectric tensor $\epsilon_{ii}(\nu)$, in turn computed for each inequivalent polarization direction according to the classical Drude-Lorentz model:

$$\epsilon_{ii}(\nu) = \epsilon_{opt} + \sum_p \frac{f_{p,ii}\nu_p^2}{\nu_p^2 - \nu^2 - i\nu\gamma_p}, \quad (7)$$

where ϵ_{opt} is the optical (high-frequency) dielectric tensor, ν_p , f_p , γ_p the frequency, oscillator strength, and damping factor for the p -th vibration mode respectively.

D. Electronic properties

Figs. 11 and 12 show (for structures #28; see Supplementary Material for the others) the electronic band structures and the DOS; the origin of energy is set at the top of the valence band. There are again differences in detail between Si and Ge, essentially confined to the conduction band, just as for the diamond structure. The valence bands show on average more similarities with lonsdaleite than with diamond⁴³: in particular the DOS is larger near the top of the valence band with a distribution covering 4 eV, and the acute maximum of the diamond structure (corresponding of course to strong s - p overlap) is far less pronounced in all the present allotropes. The same remark holds for the conduction band. The width of the valence band is reduced with respect to the diamond structure; this, and the deviation of the bonding angles with respect to the ideal tetrahedral value (see § IV F below) are clear markers of a weakened bonding; if the contributions of the s and p electrons to the DOS are computed (not shown here), we observe the quasi absence of overlap near

the top of the band (dominated by p electrons), which is of course also seen in the narrow and relatively flat profile of the top valence bands (say, from -4 to 0 eV). This is expected as all the present structures have higher values of energy than diamond: the deficit is to be found in lower bonding energies. Of interest is the structure #27 of Ge, which exhibits a low indirect band gap of barely 0.23 eV with the PBE exchange-correlation functional (see Table IV); spin-orbit correction yields a difference of 0.05 eV. While this low value of the band gap is probably also due to the well-known tendency of DFT-GGA to underestimate band gaps, it is just as well the consequence of the weakening of the s - p overlap, which suggests that some (yet unknown) phase might actually be nearly or completely metallic, as it is the case for liquid germanium⁴⁴ and amorphous metallic germanium⁴⁵. The band gaps obtained in calculations with hybrid-type functional HSE06²⁹ are also presented in the Tables (II)- (IV). Let us note that the presented values for direct (ΔE_{Γ}) and indirect band gaps were calculated using the full-electron basis set in CRYSTAL14: the computations agree reasonably well with experimental data for diamond structures in the PBE case, while they overestimate the same band gaps in the HSE case. On the contrary, computations made with VASP show that HSE computations agree well with the experimental data whereas PBE calculations strongly underestimate the same data.⁴⁶

E. Optical properties

As mentioned in the Introduction, the absorption and refraction spectra of the silicon and germanium allotropes are of interest for photovoltaic applications. For this purpose, we performed calculations of frequency-dependent dielectric functions of the new proposed allotropes, both in standard DFT and hybrid-functional frameworks. It is well-known that the former fails to reproduce the optical band gaps, especially for low-gap structures such as germanium, which is predicted to be a metal. This closing of a band gap is due to the strong correlation of d -electrons in germanium, which can be partly corrected by implementing a hybrid functional with some part of exact exchange. Hybrid functionals lead to reliable results for the band gaps of a number of elemental and binary insulators and semiconductors. In our calculations we have used the screened Heyd, Scuseria, and Ernzerhof (HSE06)²⁹ hybrid functional. We should mention that we do not pretend to describe the dielectric properties of the considered structures with high accuracy in this work, but

only to give a correct qualitative picture. Following this, we will work in the random-phase approximation and neglect local fields corrections. To make accurate predictions one needs to take into account both the local fields and excitonic effects; as is well-known, DFT is a theory based on the ground state and therefore insufficient to describe the excited states. For accurate absorption spectra with excitonic effects one has to solve the Bethe-Salpeter equation working in the GW approximation or in the framework of time-dependent DFT.

As implemented in the VASP package, the imaginary part of the frequency-dependent dielectric tensor is defined by the following formula

$$\varepsilon_{\alpha\beta}^{(2)}(\omega) = \frac{4\pi^2 e^2}{\Omega} \lim_{q \rightarrow 0} \frac{1}{q^2} \sum_{c,v,\mathbf{k}} 2w_{\mathbf{k}} \delta(\varepsilon_{c\mathbf{k}} - \varepsilon_{v\mathbf{k}} - \omega) \times \langle u_{c\mathbf{k}+\mathbf{e}_{\alpha}q} | u_{v\mathbf{k}} \rangle \langle u_{c\mathbf{k}+\mathbf{e}_{\beta}q} | u_{v\mathbf{k}} \rangle^*, \quad (8)$$

where the indices c and v refer to conduction and valence band states respectively in the sum over the empty states, $\varepsilon_{v,c\mathbf{k}}$ are the corresponding eigenenergies, Ω the volume of a primitive cell, k -point weights $w_{\mathbf{k}}$ are defined such that they sum to 1, $e_{\alpha(\beta)}$ are the unit vectors for the three Cartesian directions, and $u_{c\mathbf{k}}$ is the cell-periodic part of the orbitals at point \mathbf{k} . The real part of the dielectric tensor $\varepsilon^{(1)}$ is obtained by the usual Kramers-Kronig transformation

$$\varepsilon_{\alpha\beta}^{(1)}(\omega) = 1 + \frac{2}{\pi} P \int_0^{\infty} \frac{\varepsilon_{\alpha\beta}^{(2)}(\omega') \omega'}{\omega'^2 - \omega^2 + i\eta} d\omega' \quad (9)$$

where P denotes the principal value. By cubic symmetry, the following holds for diamond Si and Ge

$$\varepsilon_{xx}^{(1,2)} = \varepsilon_{yy}^{(1,2)} = \varepsilon_{zz}^{(1,2)}, \quad \varepsilon_{\alpha\beta}^{(1,2)} = 0, \alpha \neq \beta, \quad (10)$$

so the real and imaginary parts of the complex dielectric constant $\varepsilon = \varepsilon_1 + i\varepsilon_2$ can be determined by $\varepsilon_{1,2} = \varepsilon_{xx}^{(1,2)}$. In the present case of anisotropic structures, one can use the average values: $\varepsilon_{1,2} = \bar{\varepsilon}_{1,2} = \frac{1}{3}(\varepsilon_{xx}^{(1,2)} + \varepsilon_{yy}^{(1,2)} + \varepsilon_{zz}^{(1,2)})$.

The real (n) and imaginary (k) parts of the complex refractive index $n^* = n + ik$ define the refractive and absorption properties of a crystal, and they can be determined using the following relationships, as $\varepsilon = (n + ik)^2$:

$$n = \left[\frac{(\varepsilon_1^2 + \varepsilon_2^2)^{1/2} + \varepsilon_1}{2} \right]^{1/2} \quad (11)$$

$$k = \left[\frac{(\varepsilon_1^2 + \varepsilon_2^2)^{1/2} - \varepsilon_1}{2} \right]^{1/2}. \quad (12)$$

To check the reliability of the obtained results we have also performed the calculations for the diamond forms of Si and Ge, as experimental data for the latter is known for a long

time⁴⁷. Cubic Si and Ge have a small, 2-atomic, primitive cell and a correspondingly large BZ. To reduce the BZ we have repeated the primitive cell twice along each independent direction, introducing a supercell of $2 \times 2 \times 2$ containing $8 \times 2 = 16$ atoms: the BZ is then reduced by a factor of 2 in all directions, allowing to use half as many k -points in the calculations; this is crucial as computations with hybrid functionals are very time-consuming compared to their PBE equivalents, even more so as accurate results for optical properties require a very dense k -point mesh of the order of 2 or 3 times that typically used for relaxations. In the supercell approach just defined, a $7 \times 7 \times 7$ Gamma-centered mesh is enough; moreover, this approach eliminates the non-physical, artificial correlations arising from small fluctuations and errors in the electronic charge density on the one hand and high symmetry and small primitive cells on the other hand: for instance, by symmetry only 1/48 of the already small primitive cell of the diamond structure is required.

In the left panels of Figs. (13) and (14) are shown the calculated (red line: HSE06, blue line: PBE) and experimental⁴⁷ (black line) frequency-dependent refractive indices n of diamond Si and Ge. The absorption spectra (k) together with the reference air mass 1.5 solar spectral irradiance, given in arbitrary units, are shown in the left panels of Figs. (15) and (16). The HSE06 functional predicts the frequency dependence of n and k better than its PBE counterpart: refraction and absorption index peaks are correctly positioned for silicon, whereas for germanium there is a tendency to underestimate the experimental values; in general, we find an overall fair agreement perturbed by some oscillations.

Amorphous forms of Si and Ge, the so-called a -Si and a -Ge, their various hydrogenated forms and some Si-Ge alloys (see again Ref. 9) have shown promising properties for their use in electronics and photovoltaics, and in particular for solar cells. An accurate investigation of optical functions of amorphous Si can be found in Ref. 48; their optical spectra are characterized by one smooth absorption peak. If we compare the calculated refractive index and absorption spectra of our predicted allotropes with the corresponding spectra of amorphous forms (see the right panels of Figs. 13, 15 and Figs. 14, 16 respectively), we find a quantitative and qualitative agreement with the experimental data both in the positions and in the numerical values of the refractive and absorption peaks. This is strong evidence that our predicted allotropes can be used as a counterpart of these amorphous forms; indeed, allotrope Si #28 demonstrates prominent absorbance properties of solar light, and may thus be a promising crystalline structure for thin-film solar cells.

F. Structure and physical properties

Looking at Table V, we notice two main departures from the diamond structure: first, bond lengths are distributed around their average value in diamond (2.35 Å in Si, 2.45 Å in Ge). Second, bond angles are widely distributed around the ideal tetrahedral value of 109.47°, evocative of distorted (and thus weakened) bonding; it is as if the high-frequency phonon modes (of the bond-bending type) were actually "frozen" in the structures. This should not be surprising, given the proximity to the diamond and lonsdaleite phases, and the fact that small "topological flips" might transform the latter into the present allotropes (for instance two adjacent 6-rings may become adjacent 5- and 7-rings), see Ref. 1. The tiling approach described there can also be used, and (given the structural identities) leads to the same conclusions, namely that the structures are either columns of adamantane cages (#28 and #50), a monolayer of adamantane cages interconnected by sheets of corrugated graphene (#88), or built of lonsdaleite-like cages (also interconnected by sheets of corrugated graphene in the case of the two monoclinic allotropes #26 and #27). In other words, structures #28, #50, and #88 share more similarities with diamond than the other three, which can be seen in their systematically larger band gaps. That being said, the electronic DOS is more similar to lonsdaleite than diamond⁴³ for all the allotropes, as we have seen above, showing the limitations of structural/topological analysis alone. Exactly as for the equivalent carbon allotropes, the structures can be seen as continuous random networks, explaining why some optical properties look very much like amorphous silicon and germanium, see again 44 and 45 for the latter case.

V. SUMMARY AND CONCLUSIONS

Six new allotropes of silicon and germanium, isostructural with the six carbon allotropes studied in 1, have been investigated and their main physical properties determined by first-principles computations. While superficially similar, resulting mainly of their close proximity to their diamond/lonsdaleite parent structure, these silicon and germanium allotropes show actually some differences in detail. Severe structural distortions have as main consequence the weakening of the *s-p* overlap characteristic of the pure covalent bonding present in the diamond structures. Along with the structural similarity with the amorphous phases of Si

and Ge and the known metallic properties of Ge^{44,45}, this may suggest that some allotropes of Ge might also be metallic (even though none of those investigated here is). Finally, as seen in Figs. 4 and 5, these phases might actually be high-temperature variants, quite in agreement with the metallic behavior of liquid germanium.

ACKNOWLEDGEMENTS

The work of V.A.S., A.V.S., and D.M.P. was financially supported by the Megagrant number 14.25.31.0005 of the Russian Ministry of Education and Science. The work of V.A.S. and A.V.S. was also supported by the Ministry of Education and Science of Russia under Competitiveness Enhancement Program of the Samara National Research University for 2013-2020. The work of G.F. was supported by the Samara National Research University in the framework of Task 05B-P010-073.

APPENDIX A: THE STRUCTURE OF SUPPLEMENTARY MATERIAL

The electronic supplementary material to the paper consists of following subsections

- A. Crystallographic data for the silicon allotropes
- B. Crystallographic data for the germanium allotropes
- C. Matrices of the elastic constants C_{ab} for silicon and germanium allotropes
- D. Phonon band structure for silicon and germanium allotropes
- E. Raman shift spectra for silicon and germanium allotropes
- F. IR absorption spectra for silicon and germanium allotropes
- G. Electronic bands and DOS for silicon and germanium allotropes

* saleev@samsu.ru

† alexshipilova@samsu.ru

- [‡] davide.proserpio@unimi.it
- [§] gfadda@dmsa.unipd.it
- ¹ I. A. Baburin, D. M. Proserpio, V. A. Saleev, and A. Shipilova, *Phys. Chem. Chem. Phys.* **17**, 1332 (2015).
- ² A. R. Oganov and C. W. Glass, *J. Chem. Phys.* **124**, 244704 (2006).
- ³ A. R. Oganov, ed., *Modern Methods of Crystal Structure Prediction* (Wiley-VCH, Berlin, 2011).
- ⁴ V. A. Blatov and D. M. Proserpio, in *Modern Methods of Crystal Structure Prediction*, edited by A. R. Oganov (Wiley-VCH, Berlin, 2011) pp. 1–28.
- ⁵ V. A. Blatov, A. P. Shevchenko, and D. M. Proserpio, *Cryst. Growth Des.* **14**, 3576 (2014).
- ⁶ M. W. Deem, R. Pophale, P. A. Cheeseman, and D. J. Earl, *J. Phys. Chem.* **113**, 21353 (2009), see http://www.hypotheticalzeolites.net/DATABASE/DEEM/DEEM_PCOD/index.php.
- ⁷ M. M. J. Treacy, K. H. Randall, S. Rao, J. A. Perry, and D. J. Chadi, *Z. Kristallogr.* **212**, 768 (1997), see http://www.hypotheticalzeolites.net/DATABASE/BRONZE_CONFIRMED/index.html.
- ⁸ P. Bhubaneswari, S. Iniyar, and R. Goic, *Renew. Sust. Energ. Rev.* **15**, 1625 (2011).
- ⁹ L. El Chaar, L. A. Lamont, and N. El Zein, *Renew. Sust. Energ. Rev.* **15**, 2165 (2011).
- ¹⁰ M. Zwijnenburg, K. Jelfs, and S. Bromley, *Phys. Chem. Chem. Phys.* **12**, 8505 (2010).
- ¹¹ D. Selli, I. Baburin, R. Martanak, and S. Leoni, *Sci. Rep.* **3**, 1466 (2012).
- ¹² B. Haberl, T. Strobel, and J. Bradby, *Appl. Phys. Rev.* **3**, 040808 (2016).
- ¹³ Q. Fan *et al.*, *Appl. Phys. Rev.* **118**, 185704 (2015).
- ¹⁴ Q. Fan, J. Li, X. Peng, L. Meng, C. Tang, and J. Zhong, *Phys. Chem. Chem. Phys.* **18**, 9682 (2016).
- ¹⁵ A. Mujica, C. J. Pickard, and R. Needs, *Phys. Rev. B* **91**, 214104 (2015).
- ¹⁶ S. Botti, J. A. Flores-Livas, M. Amsler, S. Goedecker, and M. A. L. Marques, *Phys. Rev. B* **86**, 121204 (2012).
- ¹⁷ D. Y. Kim, S. Stefanoski, O. O. Kurakevych, and T. A. Strobel, *Nat. Mater.* **14**, 169 (2015).
- ¹⁸ C. Raffy, J. Furthmüller, and F. Bechstedt, *Phys. Rev. B* **66**, 075201 (2002).
- ¹⁹ B. Wen, J. Zhao, M. J. Bucknum, P. Yao, and T. Li, *Diamond Relat. Mater.* **17**, 356 (2008).
- ²⁰ <http://sacada.sctms.ru>.
- ²¹ R. Hoffmann, A. A. Kabanov, A. A. Golov, and D. M. Proserpio, *Angew. Chem. Int. Ed.* **55**, 10962 (2016).

- ²² R. Dovesi *et al.*, *Int. J. Quantum Chem.* **114**, 1287 (2014).
- ²³ R. Dovesi *et al.*, *CRYSTAL14 User's Manual*, Univ. of Torino, Torino, Italy (2014).
- ²⁴ J. P. Perdew, K. Burke, and M. Ernzerhof, *Phys. Rev. Lett.* **77**, 3865 (1996).
- ²⁵ M. F. Peitinger, D. V. Oliveira, and T. Bredow, *J. Comput. Chem.* **34**, 451 (2013).
- ²⁶ H. J. Monkhorst and J. D. Pack, *Phys. Rev. B* **13**, 5188 (1976).
- ²⁷ G. Kresse and J. Furthmüller, *Phys. Rev. B* **54**, 11169 (1996).
- ²⁸ G. Kresse and D. Joubert, *Phys. Rev. B* **59**, 1758 (1999).
- ²⁹ J. Heyd, G. Scuseria, and M. Ernzerhof, *J. Chem. Phys.* **124**, 219906 (2006).
- ³⁰ F. Birch, *Phys. Rev.* **71**, 809 (1947).
- ³¹ F. Pascale, C. Zicovich-Wilson, F. Lopez, B. Civalleri, R. Orlando, and R. Dovesi, *J. Comput. Chem.* **25**, 888 (2004).
- ³² W. M. Haynes, *CRC Handbook of Chemistry and Physics 2015-2016*, 96th ed. (CRC Press/Taylor and Francis, Boca Raton, FL, USA, 2015).
- ³³ M. Born and K. Huang, *Dynamical Theory of Crystal Lattices* (Oxford University Press, Oxford, 1954).
- ³⁴ F. Mouhat and F.-X. Coudert, *Phys. Rev. B* **90**, 224104 (2014).
- ³⁵ J. J. Gilman, *Electronic Basis of the Strength of Materials* (Cambridge University Press, Cambridge, 2003).
- ³⁶ S. Pugh, *Philos. Mag.* **45**, 823 (1954).
- ³⁷ Q. Long, X. Nie, S.-L. Shang, J. Wang, Y. Du, Z. Jin, and Z.-K. Liu, *Comput. Mater. Sci.* **121**, 167 (2016).
- ³⁸ W. Voigt, *Lehrburch der Kristallphysik* (Teubner, Leipzig, 1928).
- ³⁹ A. D. Becke and K. E. Edgecombe, *J. Chem. Phys.* **92**, 53975403 (1990).
- ⁴⁰ *Angew. Chem. Int. Ed.* **31**, 187188 (1992).
- ⁴¹ L. Kleinman, *Phys. Rev.* **128**, 2614 (1962).
- ⁴² J. Baima, A. Zelferino, P. Olivero, A. Erba, and R. Dovesi, *Phys. Chem. Chem. Phys.* (2016), 10.1039/C5CP06672G.
- ⁴³ A. De and C. E. Pryor, *J. Phys. Condens. Matter* **26**, 045801 (2014).
- ⁴⁴ J. Hafner, M. Tegze, and W. Jank, *J. Less Common Met.* **145**, 531 (1988).
- ⁴⁵ O. Shimomura, S. Minomura, N. Sakai, K. Asaumi, K. Tamura, J. Fukushima, and H. Endo, *Philos. Mag.* **29**, 547 (1974).

⁴⁶ K. Hummer, J. Harl, and K. G., Phys. Rev. B **80**, 115205 (2009).

⁴⁷ in *Optical Constants of Crystalline and Amorphous Semiconductors*, edited by A. Sadao (Springer, USA, 1999) 714th ed.

⁴⁸ A. S. Ferlauto, G. M. Ferreira, J. M. Pearce, C. R. Wronski, R. Collins, X. Deng, and G. Ganguly, J. Appl. Phys. **92**, 2424 (2002).

TABLE II. Comparison, for the diamond structure ($Fd\bar{3}m$), between the experimental and computed (CRYSTAL) values of some basic properties: cell parameters, density, bulk modulus, pressure derivative of the bulk modulus, dielectric constant, indirect and direct (at the Γ point) band gaps.

$Fd\bar{3}m$	$a, \text{\AA}$	$\rho, \text{kg m}^{-3}$	B, GPa	B'	ϵ	$\Delta E_{gap}, \text{eV}$	$\Delta E_{\Gamma}, \text{eV}$
Si, exp.	5.431	2329	98		11.7	1.12	3.4
Si, PBE/HSE06	5.414	2342	92	4.63	11.9	1.21/1.67	2.9/3.5
Ge, exp.	5.658	5323	75		16.0	0.66	0.8
Ge, PBE/HSE06	5.685	5198	67	4.86	16.2	0.52/1.05	0.7/1.24

TABLE III. The density, difference in energy from the corresponding diamond phase at zero pressure, indirect and direct (at Γ) band gaps, bulk modulus, pressure derivative of the bulk modulus, shear modulus, and static dielectric constants for the various structures of silicon.

# N , Sym. Group	#88, $Pnma$	#50, $Pnma$	#55, $Pmma$	#26, $P2/m$	#27, $C2/m$	#28, $Pbam$
$\rho, \text{kg m}^{-3}$	2293	2291	2305	2298	2291	2271
$\Delta E, \text{eV}$	0.037	0.036	0.035	0.039	0.047	0.036
$E_{gap}, \text{eV}, \text{PBE/HSE06}$	1.46/2.03	1.42/1.97	1.26/1.78	0.97/1.51	1.02/1.29	1.31/1.87
$\Delta E_{\Gamma}, \text{eV}, \text{PBE/HSE06}$	1.56/2.12	1.51/2.08	1.58/2.10	1.10/1.66	1.12/1.60	1.57/2.12
B, GPa	78	84	83	84	84	86
B'	2.74	4.31	3.75	4.14	4.35	4.64
G, GPa	48	48	48	50	51	51
$\epsilon_{xx}, \epsilon_{yy}, \epsilon_{zz}$	11.9,12.1,12.1	11.9,12.1,12.5	11.7,11.4,11.9	11.9,11.8,12.2	12.7,11.9,12.1	12.6,11.5,11.9

TABLE IV. Same properties as in Table III for the equivalent germanium allotropes

# N , Sym. Group	#88, $Pnma$	#50, $Pnma$	#55, $Pmma$	#26, $P2/m$	#27, $C2/m$	#28, $Pbam$
ρ , kg m^{-3}	5251	5086	5121	5102	5087	5054
ΔE , eV	0.037	0.038	0.036	0.044	0.052	0.033
E_{gap} , eV, PBE/HSE06	0.87/1.46	0.86/1.43	0.61/1.10	0.42/0.86	0.23/0.93	0.65/1.23
ΔE_{Γ} , eV, PBE/HSE06	0.95/1.54	0.96/1.45	1.08/1.59	0.42/0.86	0.60/1.26	0.65/1.33
B , GPa	57	59	59	59	59	60
B'	4.24	4.54	4.38	4.44	4.53	4.61
G , GPa	43	43	44	45	45	46
ε_{xx} , ε_{yy} , ε_{zz}	14.9,16.5,15.7	15.7,16.4,16.2	14.8,15.3,15.5	15.6,15.9,15.5	16.7,17.8,16.8	16.1,14.9,15.5

TABLE V. Bond lengths and angles, and shortest non-bonding distances in Si and Ge allotropes.

Structure	Bond lengths, \AA	Bond angles, degrees	Shortest non-bonding distance, \AA
Si#26	2.308-2.382	95.98-126.34	3.818
Si#27	2.308-2.415	95.31-125.84	3.820
Si#28	2.308-2.406	93.14-124.12	3.818
Si#50	2.301-2.386	96.95-127.46	3.826
Si#55	2.322-2.422	97.91-120.04	3.828
Si#88	2.322-2.380	98.16-119.32	3.837
Ge#26	2.436-2.562	94.76-126.16	4.055
Ge#27	2.436-2.533	94.76-126.16	4.055
Ge#28	2.447-2.539	92.88-120.79	4.057
Ge#50	2.439-2.530	96.29-122.11	4.067
Ge#55	2.451-2.547	98.65-119.12	4.058
Ge#88	2.459-2.514	97.51-120.61	4.068

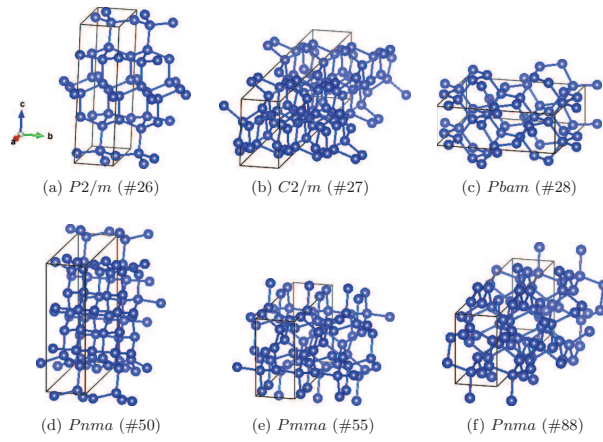


FIG. 1. Perspective view of the silicon allotropes #26, #27, #28, #50, #55, and #88.

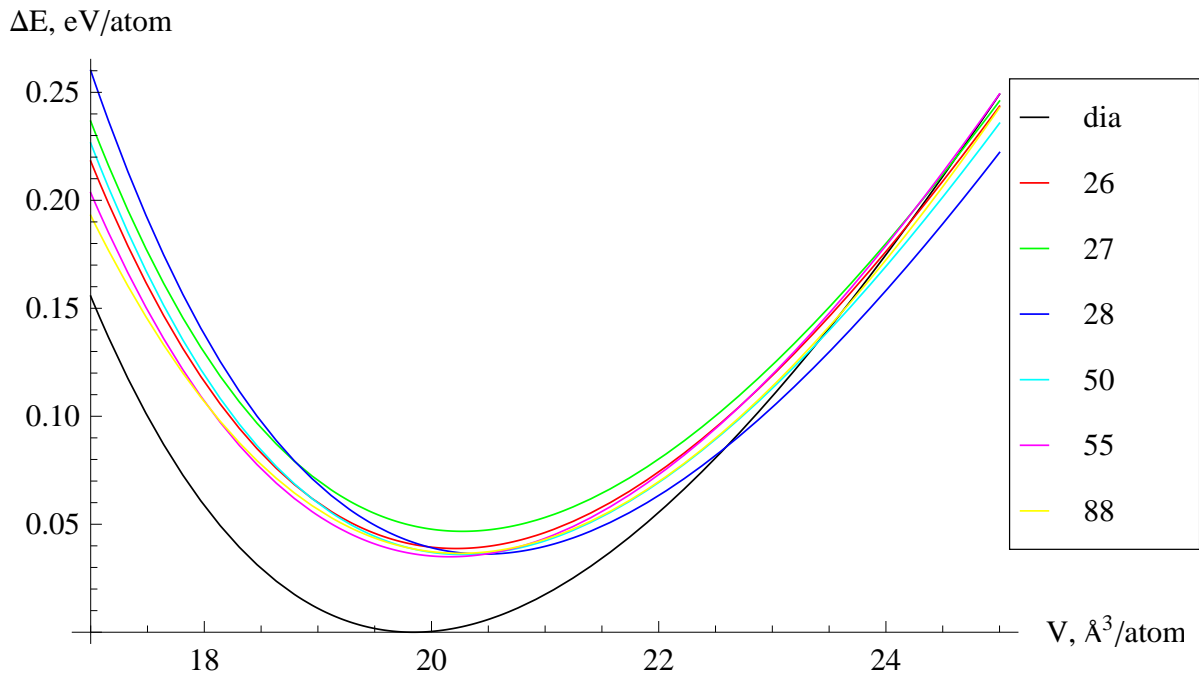


FIG. 2. Energy per atom as a function of volume for silicon allotropes.

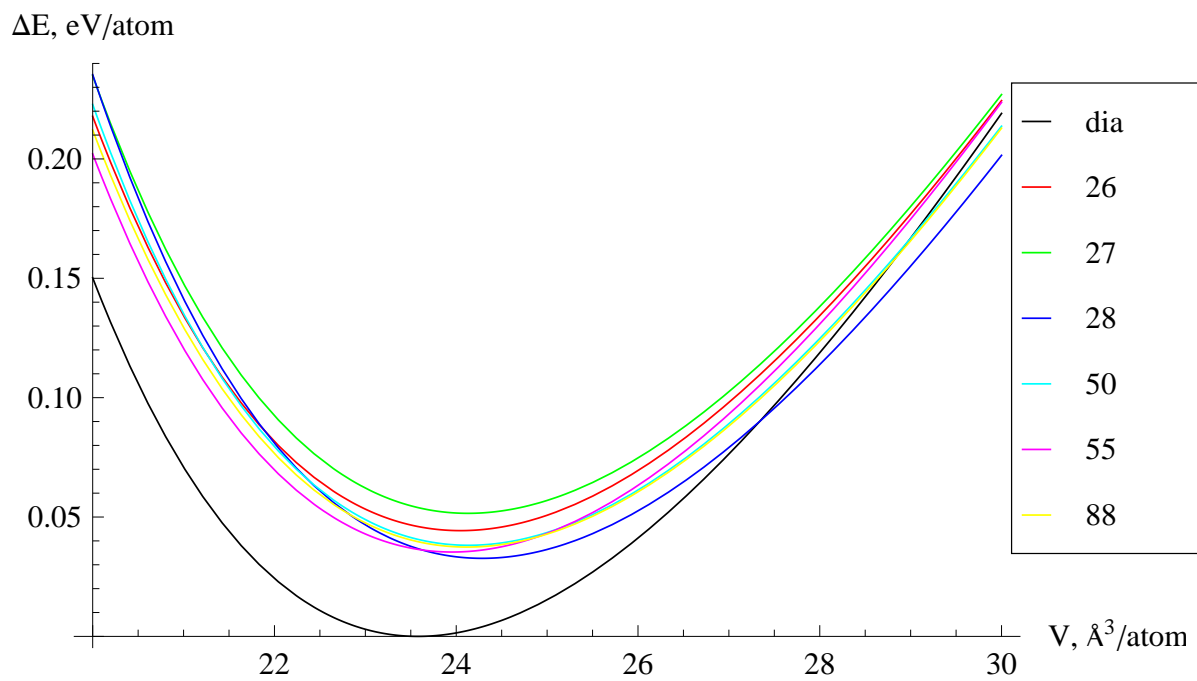


FIG. 3. Energy per atom as a function of volume for germanium allotropes.

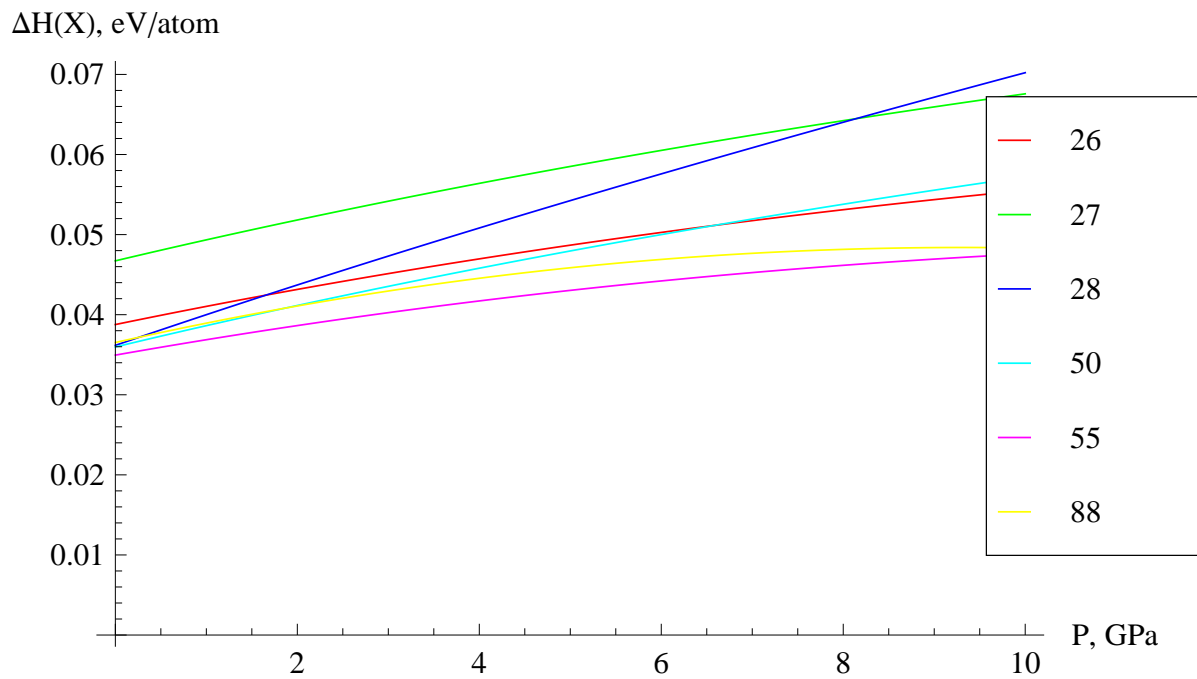


FIG. 4. Enthalpy difference $\Delta H(P)$ per atom as a function of pressure for silicon allotropes.

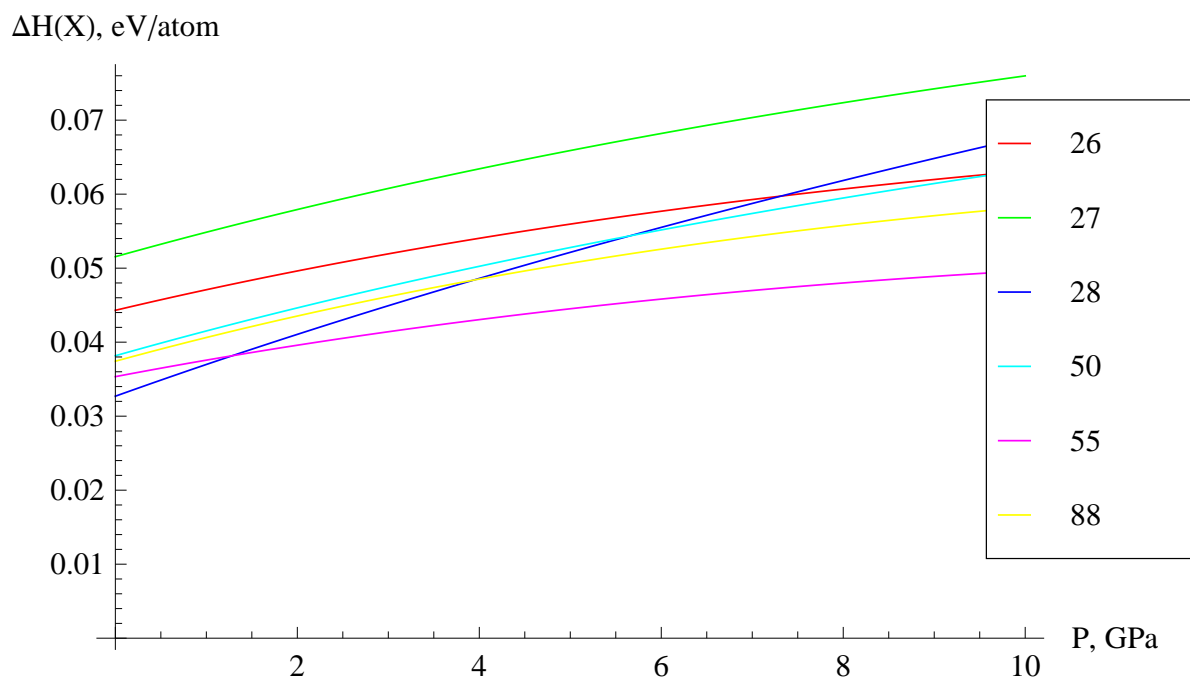


FIG. 5. Enthalpy difference $\Delta H(P)$ per atom as a function of pressure for germanium allotropes.

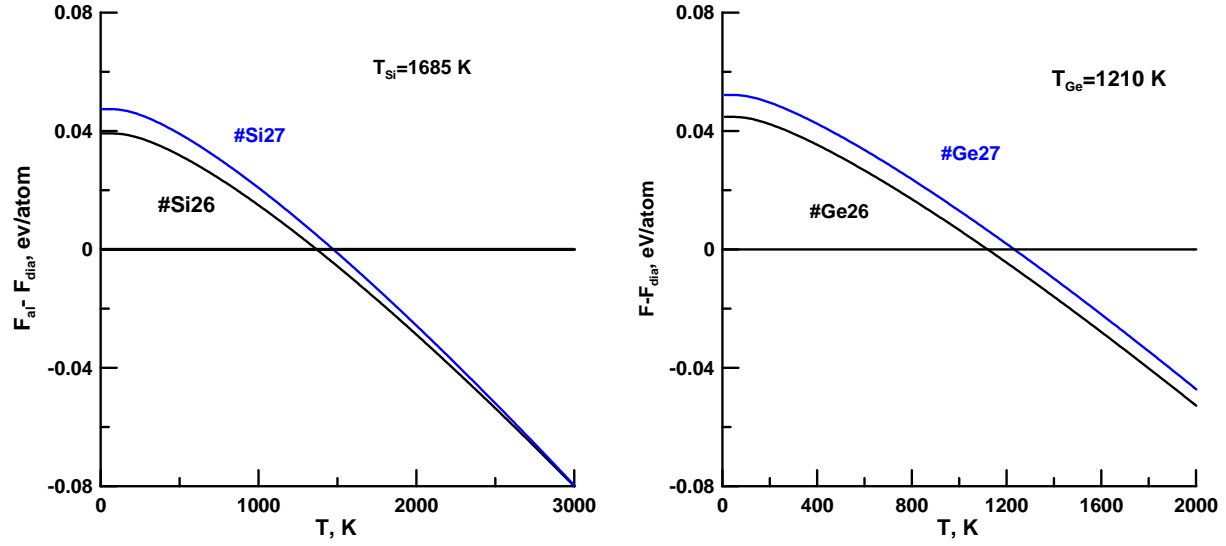


FIG. 6. Free energy difference $\Delta F(T)$ per atom as a function of absolute temperature for silicon (left panel) and germanium (right panel) allotropes #26 and #27.

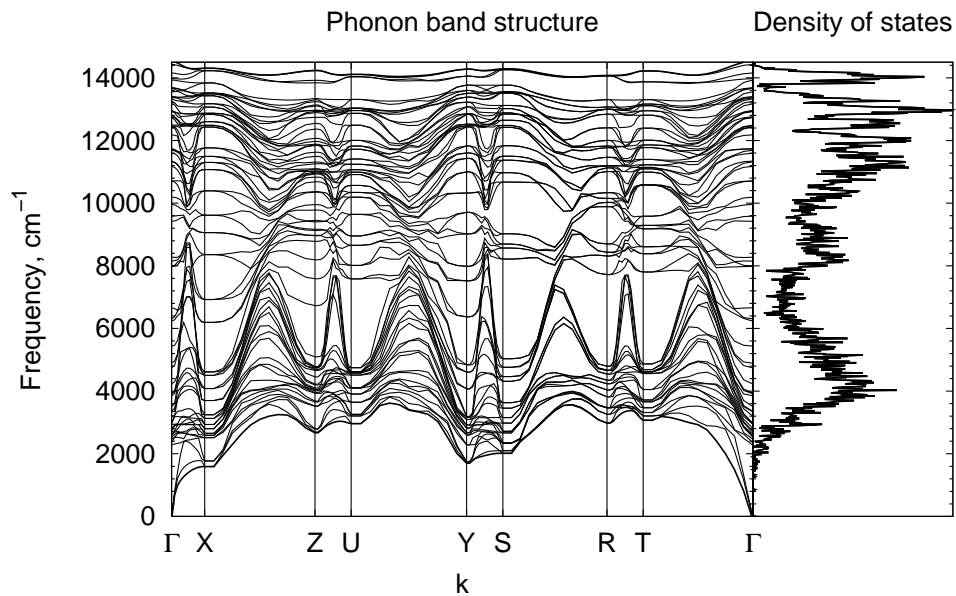


FIG. 7. Phonon band structure and DOS for silicon allotrope Si#28.

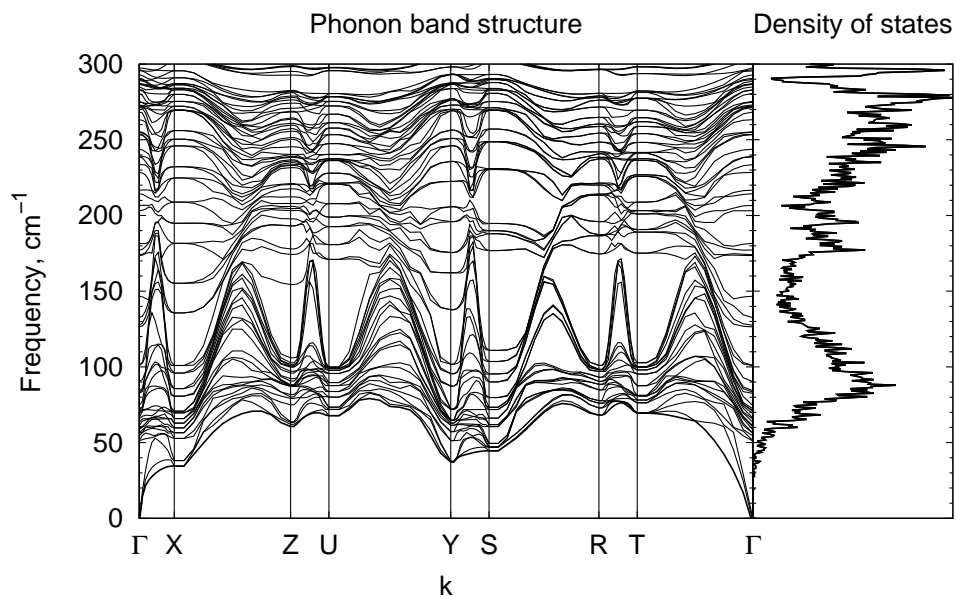


FIG. 8. Phonon band structure and DOS for germanium allotrope Ge#28.

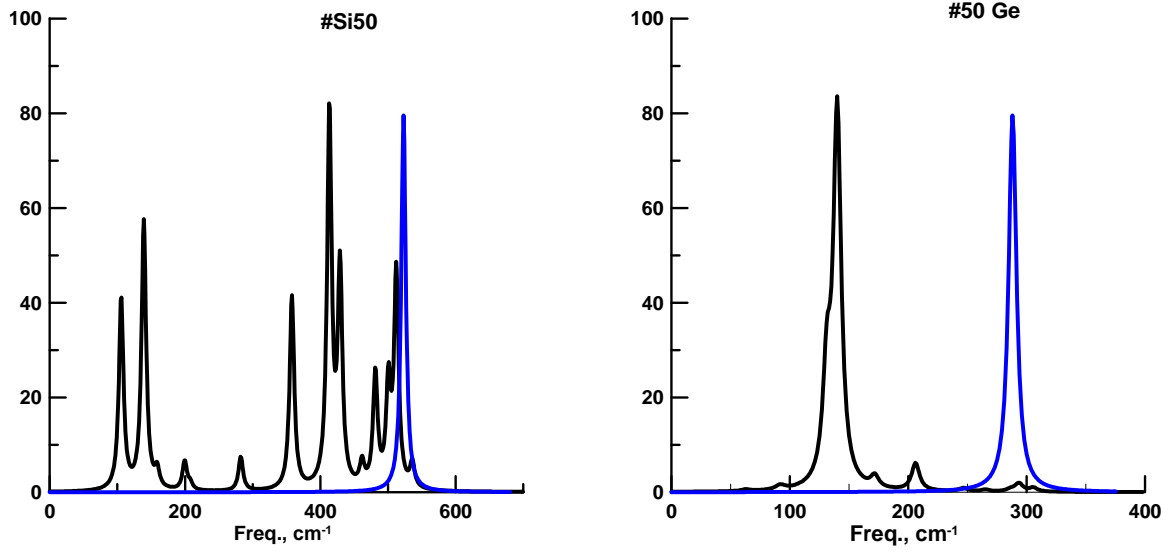


FIG. 9. Raman shift spectra for silicon (left panel) and germanium (right panel) allotropes #50 (black lines) and diamond structures (blue lines).

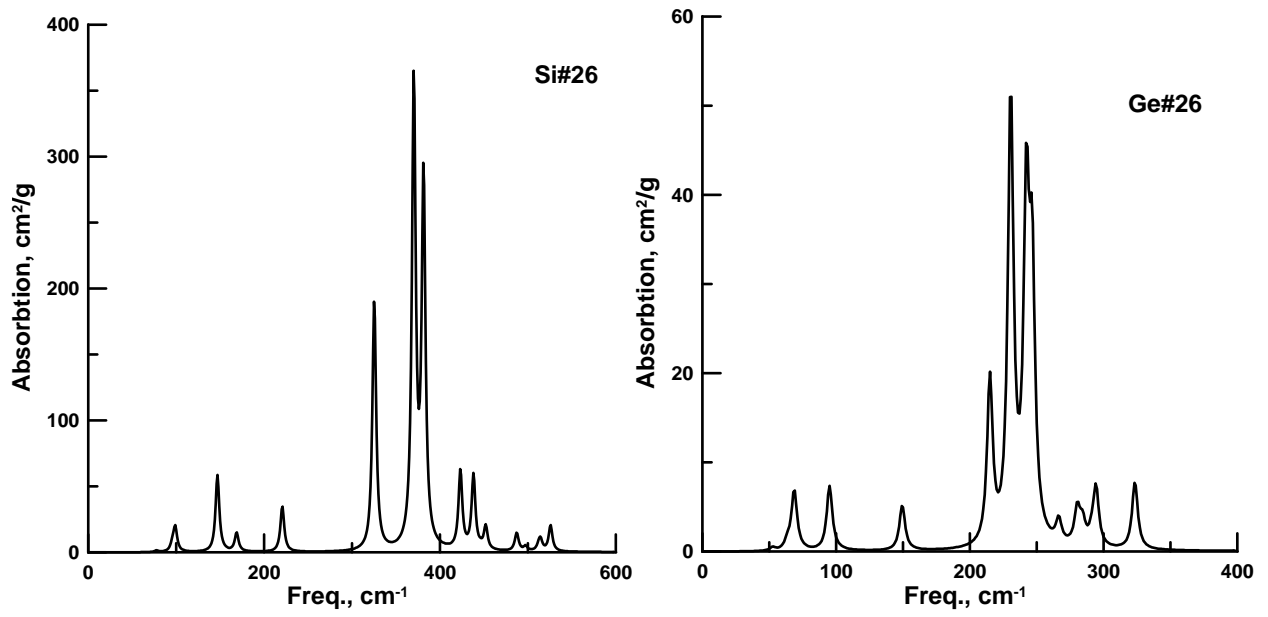


FIG. 10. IR absorption spectra for silicon (left panel) and germanium (right panel) allotropes #26 (black line) .

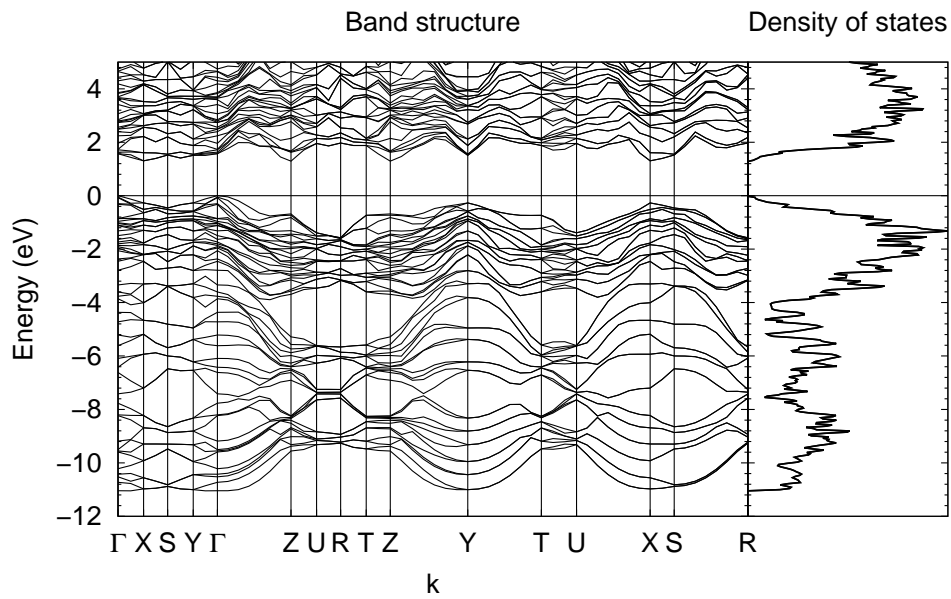


FIG. 11. Electronic band structure and DOS for silicon allotrope Si#28.

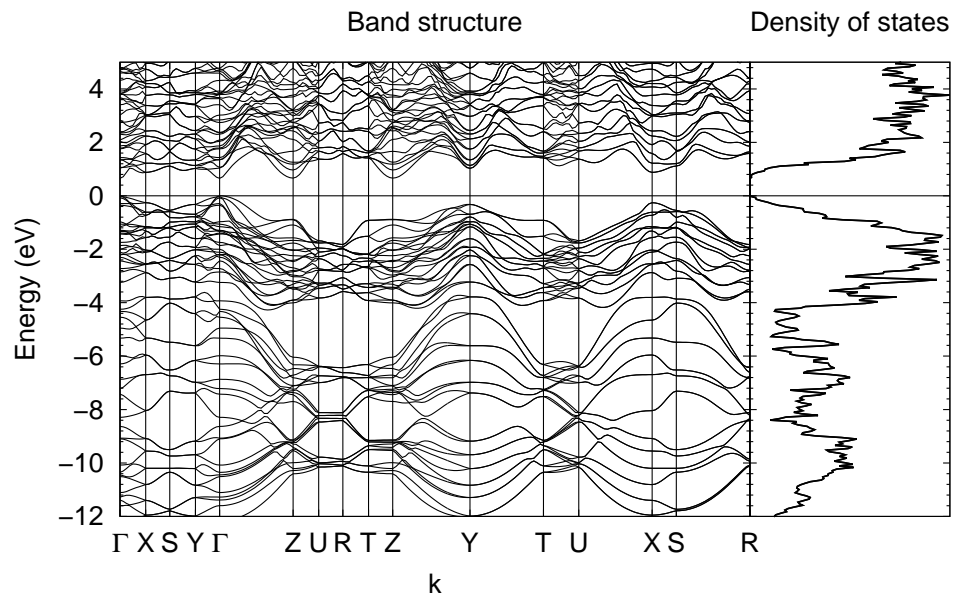


FIG. 12. Electronic band structure and DOS for germanium allotrope Ge#28.

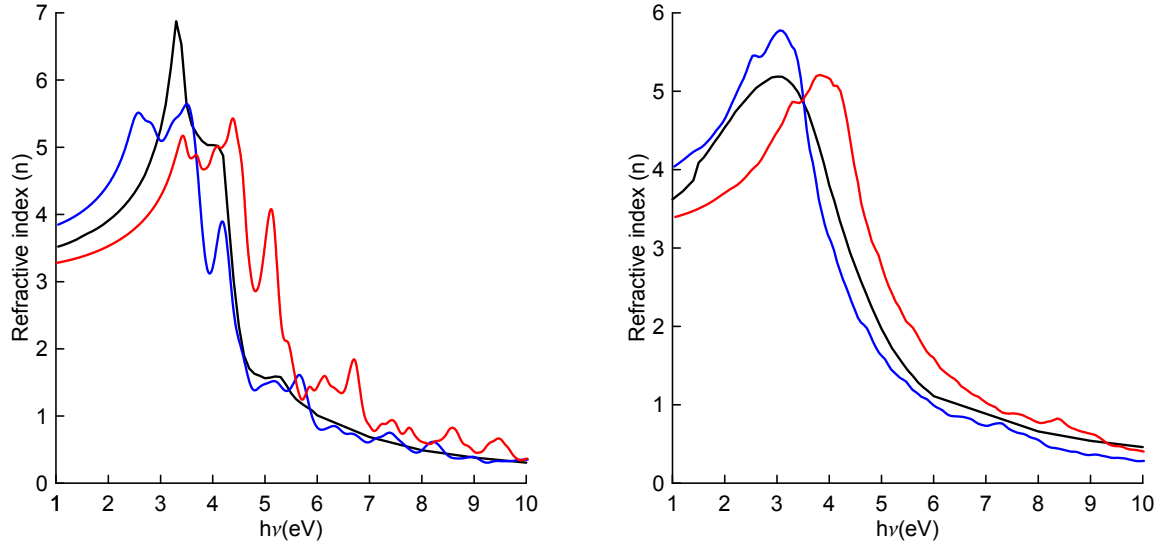


FIG. 13. Real part of the refractive index (n) for Si diamond (left panel) and Si#28 (right panel) as a function of photon energy. Black line – experiment, blue line – results obtained with PBE functional, red line – results obtained with HSE06 functional.

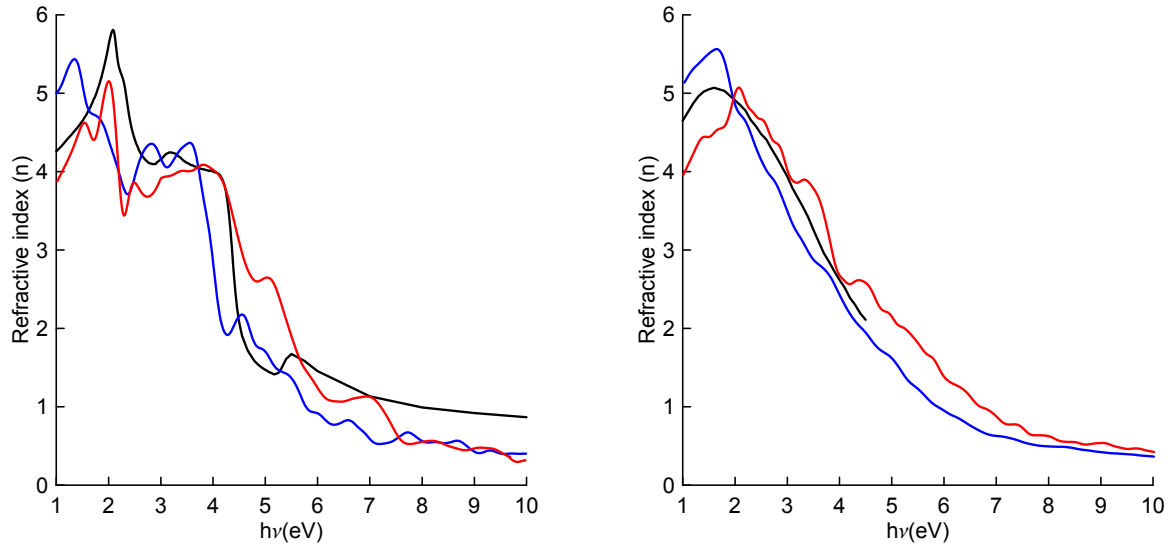


FIG. 14. Real part of the refractive index (n) for Ge diamond (left panel) and Ge#28 (right panel) as a function of photon energy. Same legend as in Fig. 13.

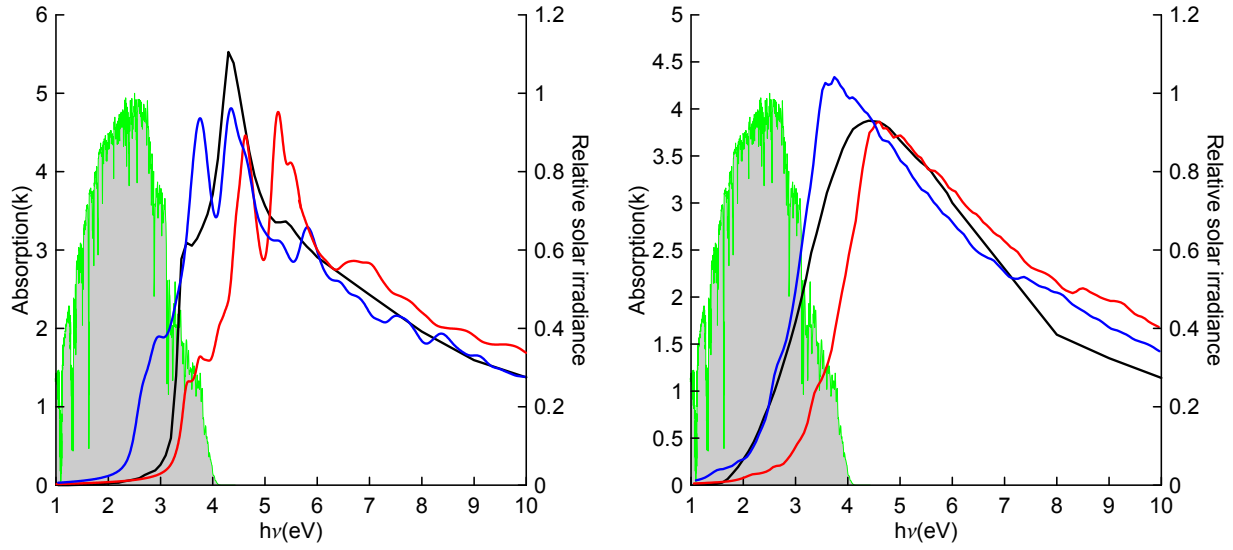


FIG. 15. Imaginary part of the refractive index (k) for Si diamond (left panel) and Si#28 (right panel) as a function of photon energy. Black line – experiment, blue line – results obtained with PBE functional, red line – results obtained with HSE06 functional. Green line with shaded area – reference air mass 1.5 solar spectral irradiance.

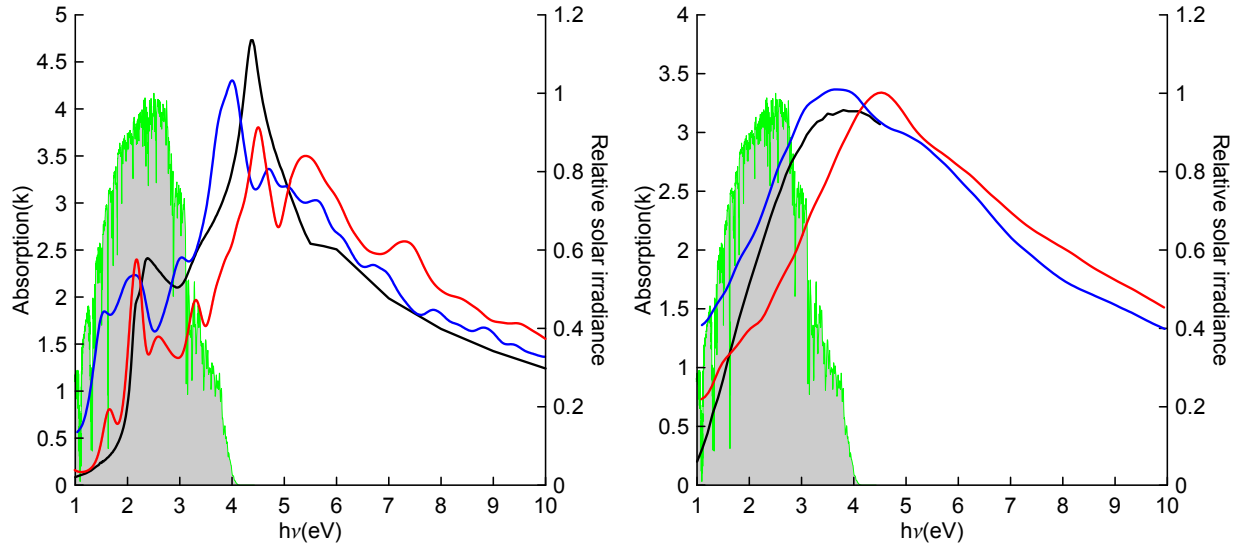


FIG. 16. Imaginary part of the refractive index (k) for Ge diamond (left panel) and Ge#28 (right panel) as a function of photon energy. Same legend as in Fig. 15.